

pubs.acs.org/NanoLett Letter

# Enhancing Intracellular Optical Performance and Stability of Engineered Nanomaterials via Aqueous Two-Phase Purification

Aceer Nadeem, Aidan Kindopp, Ian Wyllie, Lauren Hubert, James Joubert, Sophie Lucente, Ewelina Randall, Prakrit V. Jena, and Daniel Roxbury\*



Cite This: https://doi.org/10.1021/acs.nanolett.3c01727



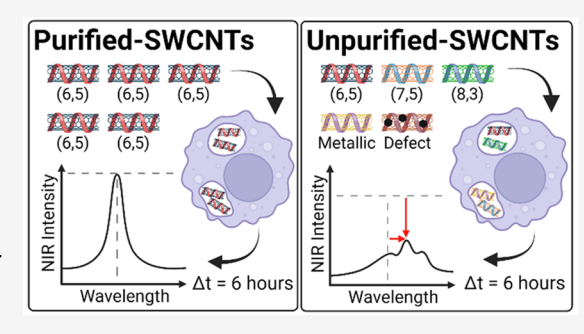
**ACCESS** I

III Metrics & More

Article Recommendations

s Supporting Information

ABSTRACT: Supramolecular hybrids of DNA and single-walled carbon nanotubes (SWCNTs) have been introduced in numerous biosensing applications due to their unique optical properties. Recent aqueous two-phase (ATP) purification methods for SWCNTs have gained popularity by introducing specificity and homogeneity into the sensor design process. Using murine macrophages probed by near-infrared and Raman microscopies, we show that ATP purification increases the retention time of DNA-SWCNTs within cells while simultaneously enhancing the optical performance and stability of the engineered nanomaterial. Over a period of 6 h, we observe 45% brighter fluorescence intensity and no significant change in emission wavelength of ATP-purified DNA-SWCNTs relative to



as-dispersed SWCNTs. These findings provide strong evidence of how cells differentially process engineered nanomaterials depending on their state of purification, lending to the future development of more robust and sensitive biosensors with desirable *in vivo* optical parameters using surfactant-based ATP systems with a subsequent exchange to biocompatible functionalization.

KEYWORDS: aqueous two-phase purification, near-infrared fluorescence, nanoparticle optical stability, biosensing, nanoparticle exocytosis

Biomedical research has been enhanced by the discovery of novel nanoparticles that can be functionalized and used in various bioimaging, biosensing, and drug delivery applications. Single-walled carbon nanotubes (SWCNTs), i.e. one type of carbon-based nanoparticle, are effectively one-dimensional materials that have been the focus of numerous biomedical studies due to their unique physicochemical and optical properties. SWCNTs are innately hydrophobic and require chemical functionalization to be compatible at the "nanobio" interface. To allow for enhanced biocompatibility of these nanoparticles while maintaining their intrinsic optical properties, amphiphilic polymers such as single-stranded DNA can be complexed with SWCNTs to form solubilized DNA-SWCNT hybrids. Other functional SWCNT wrappings include peptides, polymers, and various surfactants. 12,13

Semiconducting SWCNTs exhibit photoluminescence (fluorescence) that is inherently photostable, <sup>14</sup> is emitted in the near-infrared (NIR) spectrum, <sup>15</sup> and is responsive to their local environment. <sup>16</sup> A typical sample of as-produced (raw) SWCNTs contains differing species (chiralities) which are denoted based on their chiral indices (*n*,*m*). <sup>17,18</sup> The existence of multiple chiralities within a sample of SWCNTs allows for multiplexed bioimaging where many proteins, cells, or tissues may be labeled at once. <sup>19</sup> Whereas conventional fluorescence dyes may only be able to accurately distinguish 4–5 colors, SWCNT samples allow for simultaneous imaging of 17 different colors using hyperspectral imaging. <sup>20</sup> Based on *in* 

vitro or in vivo conditions, the innate fluorescence of SWCNTs has been shown to shift in intensity and/or center wavelength. 14,21,22 Recently, functionalized SWCNTs have been used to detect lipid accumulations within live cells and animals, 23 track biochemical information via SWCNT-integrated wearable textiles, 24 and detect the presence of E. coli to aid in food safety monitoring. 25 However, raw samples of SWCNTs with their vast composition of chiralities, carbonaceous, 26 and inorganic impurities 27 may subject cells to increased levels of cytotoxicity 28 and fluorescence quenching interactions in biological environments, 29 motivating researchers to devise methods to purify samples of SWCNTs.

Polymer–polymer aqueous two-phase (ATP) systems, with studies dating back five decades,<sup>30</sup> is a biphasic, liquid–liquid extraction technique used to purify a wide array of biological and chemical species.<sup>31–33</sup> In comparison to other sorting methods, polymer–polymer ATP systems benefit from being scalable, environmentally conscious, and inexpensive.<sup>34,35</sup> ATP purification methods have been employed to resolve SWCNTs

Received: May 9, 2023 Revised: June 30, 2023



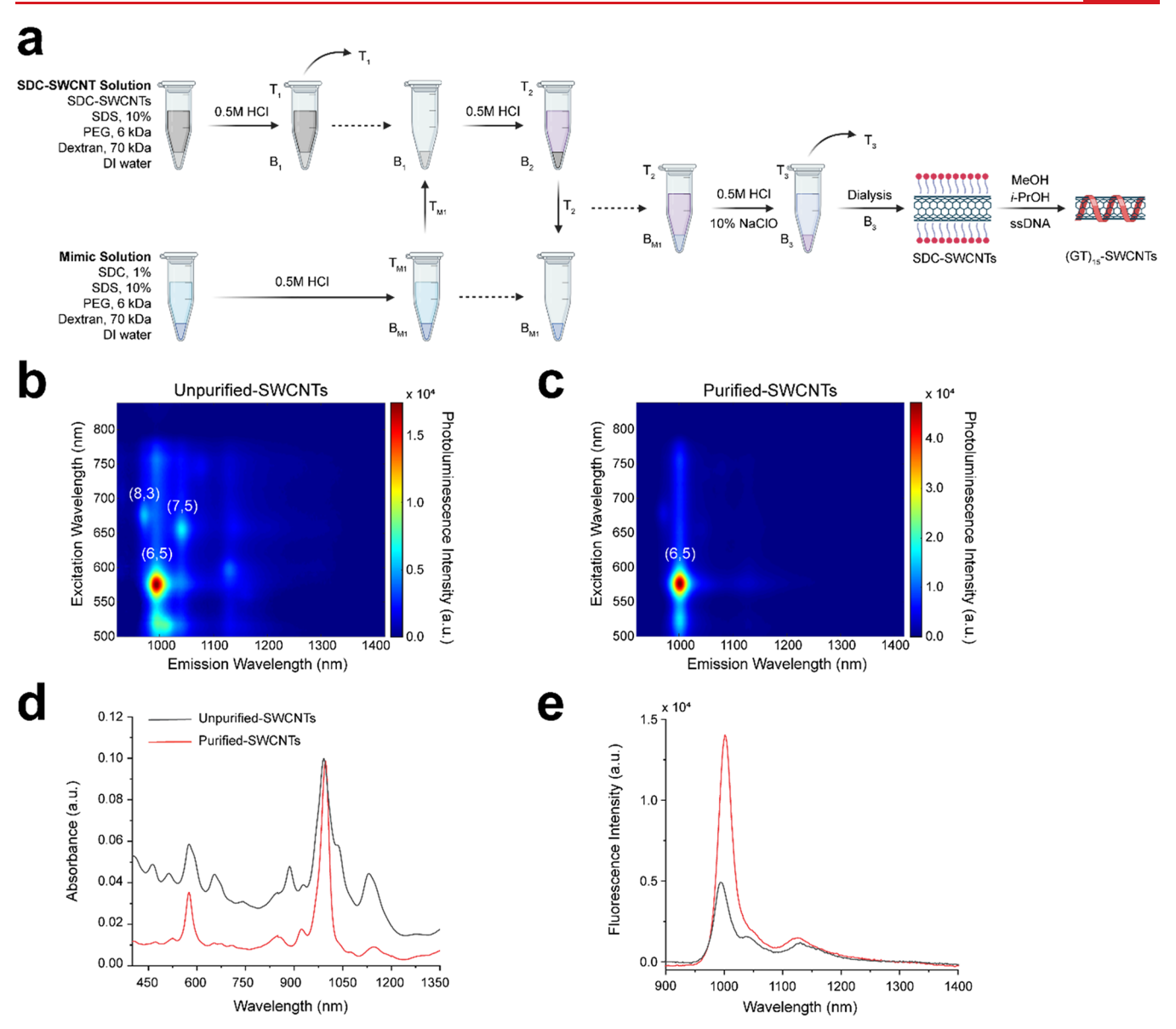


Figure 1. Preparation and characterization of DNA-SWCNT samples. (a) Schematic depicting the method for the aqueous two-phase (ATP) purification and surface exchange from SDC to DNA of (6,5) purified SWCNTs from a raw SWCNT sample. Two-dimensional photoluminescence plots of (b) unpurified and (c) purified DNA-SWCNTs. (d) Absorbance of unpurified-SWCNTs and purified-SWCNTs diluted to match absorbance (0.10 AU) at 990 nm and (e) NIR fluorescence spectra measured at equal values of  $A_{990 \text{ nm}}$  (1.0 AU) using a 575 nm excitation source.

by chirality and/or enantiomer as well as to remove aggregates and impurities; <sup>36</sup> however, current challenges include overcoming interfacial trapping, i.e. a species of interest becoming trapped between the top and bottom phases, and reducing experimental complexity. <sup>37</sup> Lyu et al. reported a 14-step ATP process with the ability to purify up to four SWCNT chiralities from a single dispersion simultaneously while preventing interfacial trapping. <sup>38</sup> Following this, Li et al. were able to decrease experimental complexity with their simplified 3-step process to resolve 11 different SWCNT chiralities and enantiomers using a cosurfactant mixture. <sup>39</sup> Most recently, Nißler et al. expanded upon the work to create monochiral, multiplexed, and ratiometric biosensors for dopamine and riboflavin via a surface exchange from surfactant-coated to ssDNA-functionalized SWCNTs. <sup>19,40</sup>

With proper functionalization, such as with a DNA wrapping, SWCNTs are readily endocytosed into cells and enter the endosomal pathway for subsequent processing.<sup>41</sup> The

SWCNTs remain brightly fluorescent within live cells and animals for extended periods of time, thus achieving long-term bioimaging and biosensing. 42 We have previously shown that their spectral modulations are indicative of the environment that they experience within the cells and can report the type of endosomal compartment within which they reside. 43 However, these spectral modulations which previous sensors are built upon are intrinsic to the system due to heterogeneity within nonpurified SWCNTs. Therefore, is it possible to formulate a novel *in vitro* biosensing platform using single-chirality purified SWCNTs where optical stability is the expectation under normal conditions and any significant deviations can be directly attributed to an external disturbance?

Here, utilizing recently demonstrated ATP purification methods of SWCNTs, we investigate and compare the uptake and retention, intracellular stability of optical properties, and cytotoxic effects of both ATP-sorted and as-dispersed DNA-functionalized SWCNTs in RAW 264.7 murine macrophages.

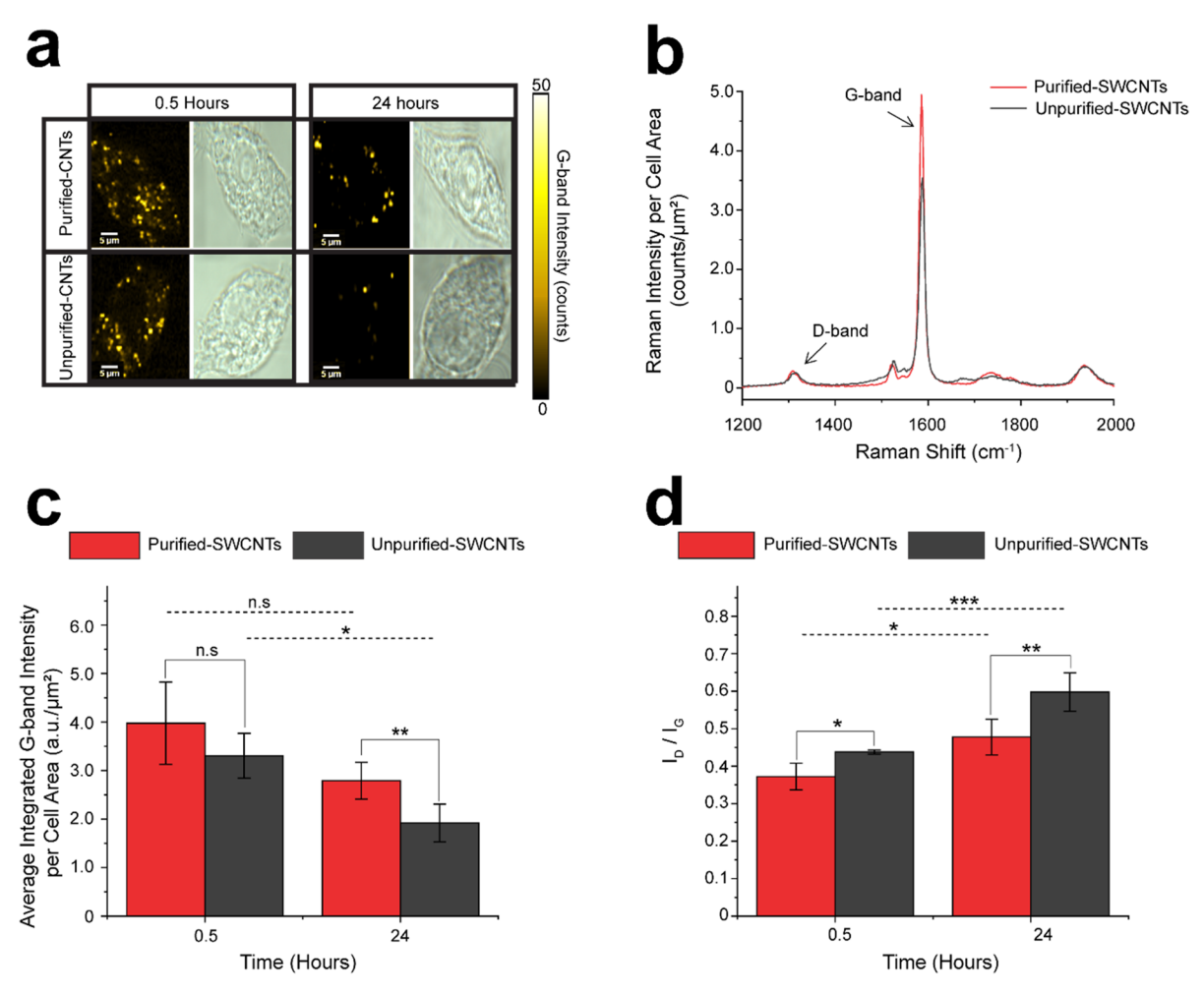


Figure 2. DNA-SWCNT uptake and retention via confocal Raman microscopy. (a) G-band intensity maps and transmitted light images of intracellular purified- and unpurified-SWCNT samples at 0.5 and 24 h after the pulse incubation. (b) Raman spectra of purified- and unpurified-SWCNT samples normalized by cell area at 0.5 h. (c) Bar graph of intracellular G-band intensity per cell area for each sample at 0.5 and 24 h. (d) Bar graph of D-band to G-band ratios for each sample at 0.5 and 24 h. Bars in (c) and (d) represent the mean, and whiskers represent standard deviation for each condition ( $n \ge 5$  cells per condition). Two-sample t-tests were performed between different samples and between different time points (\*\*\*p < 0.001, \*\*p < 0.01, and \*p < 0.05).

Dosing the cells with equal concentrations of either ATP-sorted or as-dispersed SWCNTs resulted in a statistically identical uptake. However, we found that the ATP-sorted SWCNTs were highly retained by macrophages over the course of 24 h, whereas the intracellular content of as-dispersed SWCNTs decreased significantly. Moreover, in stark contrast to as-dispersed SWCNTs, the *in vitro* spectral stability of ATP-sorted SWCNTs showed no significant decrease in fluorescence intensity or change in center wavelength over the course of 6 h. Finally, we observed no significant deleterious effects on cell health for neither the ATP-sorted nor the as-dispersed SWCNTs. These findings demonstrate the manner in which advanced SWCNT purification and homogenization methods can enable several distinct advantages in bioimaging and biosensing applications.

Samples of as-dispersed (unpurified) and ATP-sorted (purified) SWCNTs were prepared via probe-tip sonication with an amphiphilic polymer, followed by ultracentrifugation. Unpurified-SWCNTs were dispersed directly with single-stranded (GT)<sub>15</sub> DNA and used as prepared. In contrast, purified-SWCNTs were initially dispersed in sodium deoxycholate (SDC) and subjected to an ATP sorting procedure,

and then the SDC surfactant coating was exchanged for  $(GT)_{15}$  ssDNA. The method used, first developed by Li et al., separates the (6,5)-SWCNT from the bulk phase by exploiting differences in the diameters of each SWCNT chirality (Figure 1a).<sup>39</sup> After the first step in the ATP process, the successful separation of a (6,5)-/(7,4)-purified layer was qualitatively confirmed by the distinctive purple color of the T2 phase (Figure S1b). 44 The (6,5)-/(7,4)-purified T<sub>2</sub> phase was further processed to remove the (7,4)-SWCNT species, leaving behind a (6,5)-SWCNT-enriched B<sub>3</sub> phase. To confirm the chiral compositions of the unpurified- and purified-SWCNT samples, two-dimensional photoluminescence excitationemission plots were generated for each sample. As expected for the unpurified sample, the (6,5)-SWCNT dominates the photoluminescence plot at 995 nm, but there are many other chiralities present as well (Figure 1b). An analysis of the purified-SWCNT photoluminescence plot proves successful purification of the (6,5)-SWCNT in the ATP process (Figure 1c), with the extraction achieving a purity of >95% as quantified by the ratio between the (6,5)-SWCNT peak intensity versus the summation of intensities over every other excitation and emission wavelength.

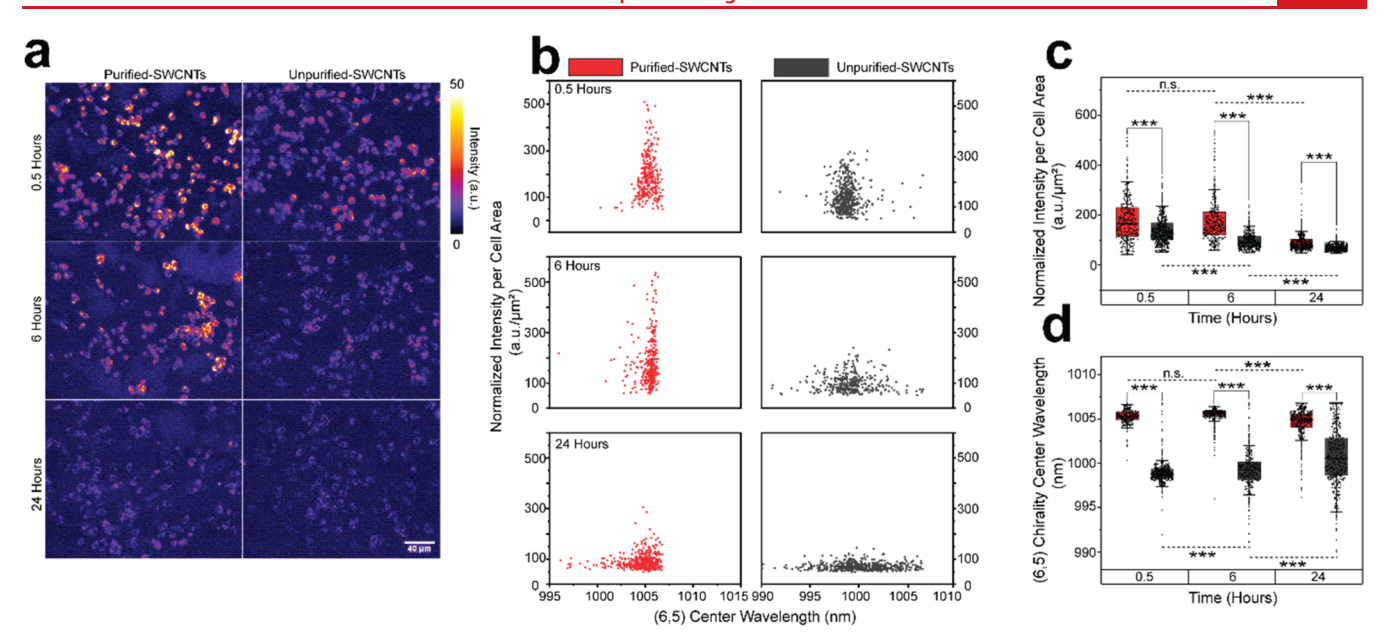


Figure 3. Purity-dependent intracellular optical performance of DNA-SWCNTs. (a) NIR fluorescence images for both purified-SWCNTs and unpurified-SWCNT samples from 0.5 to 24 h. (b) ROI scatter plot of normalized NIR fluorescence intensity vs (6,5)-SWCNT center wavelength for both purified-SWCNTs and unpurified-SWCNT samples over 24 h. (c) NIR fluorescence intensity per cell area from individual RAW 264.7 macrophage cells as a function of the time after internalization and DNA-SWCNT sample purity. (d) (6,5)-SWCNT center wavelength for each ROI as a function of time and sample purity after cellular internalization. For both (c) and (d), a minimum of  $n \ge 150$  cells per condition were analyzed. The boxes represent 25–75% of the data, horizontal lines represent medians, and whiskers represent mean  $\pm$  standard deviation. A two-sample t-test was performed between different samples and different time points (\*\*\*p < 0.001).

The ATP process produces a (6,5)-SWCNT purified sample with an unknown extinction coefficient, which poses difficulty when determining the concentration of the sample.<sup>45</sup> Because (6,5)-SWCNT is the primary chirality in each sample, the total concentrations of the samples are highly correlated to the absorbance peak of the (6,5)-SWCNT chirality, found near the absorbance value at 990 nm  $(A_{990 \text{ nm}})$ . Moreover, an absorbance value of 1.0 AU at  $A_{990\,\mathrm{nm}}$  has been shown to correlate to a concentration of approximately 10 mg L<sup>-1</sup> for CoMoCat SWCNTs. 46 For both the unpurified-SWCNT and purified-SWCNT samples, a dilution factor was calculated to reach a value of 0.10 AU at A<sub>990 nm</sub> (Figure 1d). An A<sub>990 nm</sub> value of 0.10 AU correlates to approximately 1 mg L<sup>-1</sup>, which is within the concentration range that is nontoxic to cells while still emitting enough fluorescence for subsequent intracellular investigation.4

A fluorescence solution spectrum was taken with a 575 nm laser excitation source for each sample at the same  $A_{990\,\mathrm{nm}}$  value of 1.0 AU (Figure 1e). When the (6,5)-SWCNT emission peak from the purified-SWCNT at 1001 nm is compared to that of the unpurified-SWCNT sample at 994 nm, the purified-SWCNT solution peak is 285% brighter with the same amount of (6,5)-SWCNT present. This observation can likely be attributed to the removal of nonfluorescent metallic SWCNTs and other carbonaceous impurities which can quench the emission of semiconducting chiralities in solution. The (6,5)-SWCNT emission peak in the purified-SWCNT solution is also red-shifted by 7 nm as compared to the unpurified-SWCNT solution.

A thorough investigation into the fundamental differences between each sample was conducted to probe this apparent shift in the emission wavelength. First, atomic force microscopy (AFM) imaging was performed and found no significant difference in the mean lengths between unpurified

and purified SWCNTs (Figure S3). Next, circular dichroism (CD) spectroscopy confirmed that no significant enantiomeric separation occurred during the ATP process (Figure S4). X-ray photoelectron spectroscopy showed that purified-SWCNTs have more carbon-oxygen C 1s bonds compared to unpurified-SWCNTs (Figure S5 and Table S1). Finally, solution-phase Raman spectroscopy showed that purified SWCNTs have a significantly lower  $I_D/I_G$  ratio than unpurified-SWCNTs, meaning that purified-SWCNTs have fewer sp<sup>3</sup> defects per nanotube (Figures S6 and S11). These results indicate that oxygen is being incorporated into the sp<sup>2</sup> carbon lattice. We hypothesize that oxygen atoms in the SWCNT lattice cause a decrease in exciton energy, resulting in a red-shifted emission peak. Previous work with SWCNTs seems to show slight red shifting in photoluminescence plots at the (6,5)-SWCNT emission peak after exposure to a sp<sup>3</sup> oxygen doping technique<sup>48</sup> which likely also added oxygen atoms into the sp<sup>2</sup> carbon lattice. Through an analysis of photoluminescence plots, absorption spectra, solution spectra, and additional surface chemistry characterization, we conclude that the aqueous two-phase purification of the (6,5)-SWCNT chirality from SG65i CoMoCat SWCNTs was successful and that the samples are ready for intracellular investigation.

The two different DNA-SWCNT samples were introduced into a model mammalian cell line (i.e., RAW 267.4 murine macrophages) to investigate how the purity of the sample influences their interactions within a biological system. Macrophages were chosen as the cell type for this experiment because they are biologically relevant, as they are the first cells to process foreign bodies and nanoparticles in systemic circulation. We applied confocal Raman microscopy to observe sample-dependent uptake, intracellular processing, and exocytosis for both unpurified and purified DNA-SWCNT samples. Cells were dosed with 1 mg  $\rm L^{-1}$  of either sample for 30 min,

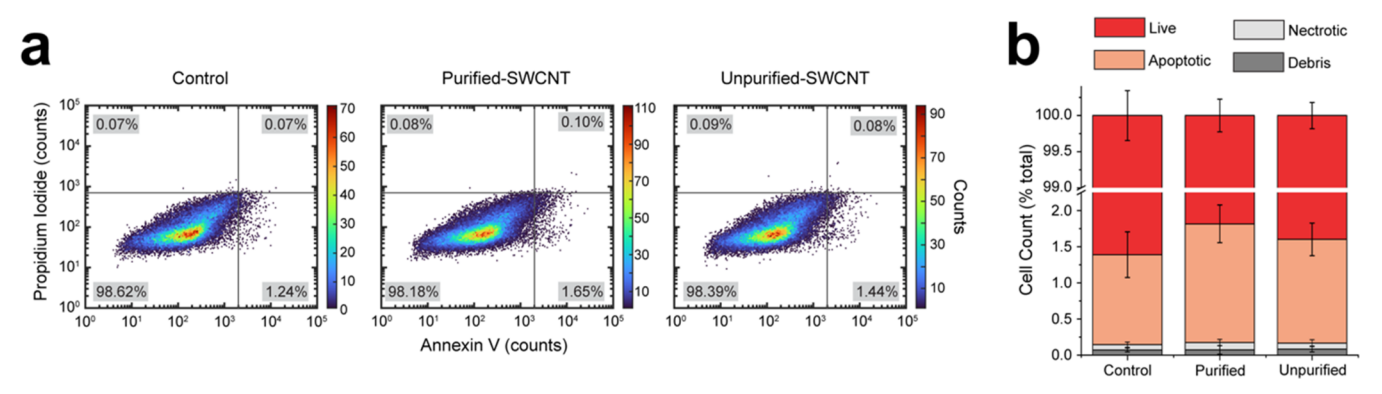


Figure 4. Cell viability assay to assess cytotoxic effects. (a) Scatter plots for Annexin V/PI viability assay after 24 h of continuous culture in a 1 mg  $L^{-1}$  SWCNT solution, and (b) bar graphs of quadrants from plots in (a) where error bars represent the standard deviation.

washed, and then placed in fresh media for 30 min or 24 h, after which the cells were fixed and placed in phosphate buffered saline (1xPBS) for confocal Raman microscopy.

Raman images were acquired from individual cells at a 100× magnification to investigate the G-band, a Raman feature of SWCNTs which linearly scales with SWCNT concentration, 42,49 and the D-band to G-band ratio, which correlates to the amount of impurities and defects in SWCNTs. 50,51 G-band intensity images were constructed next to transmitted light images for each cell condition (Figure 2a). A stronger reduction in intensity of the unpurified-SWCNT sample can be observed at 24 h when compared to the purified-SWCNT sample. Figure 2b provides the spectra of the same cells shown in Figure 2a at 30 min. The SWCNT uptake and retention by cells were quantified as the integrated G-band intensity per cell area (Figure 2c). No significant difference was observed in the uptake of either SWCNT sample, i.e., the 30 min time point, signifying that nanoparticle uptake by macrophages was independent of sample purity. However, while the G-band intensity of the purified-SWCNT sample did not significantly decrease over the course of 24 h, there was a 30% decrease in the unpurified-SWCNT sample. This is in alignment with our previous findings<sup>42</sup> and confirms that exocytosis of the unpurified-SWCNT sample is more rapid as compared to that of purified-SWCNTs. Furthermore, at both 30 min and 24 h time points, the purified-SWCNT sample has a significantly lower integrated D-band to G-band ratio as compared to the unpurified-SWCNT (Figure 2d). We correlate this to the purified-SWCNT sample having significantly fewer impurities and defects. This further supports our hypothesis that the number of defects and impurities in a sample can influence the degree of exocytosis; i.e., having a higher quantity of impurities and defects in a sample will cause the cell to expel the SWCNTs more rapidly. Interestingly, the D-band to G-band ratio increases over time for both samples, suggesting that cellular enzymes are possibly creating defects on the SWCNT This hypothesis is supported by in vitro experimentation, in which 24 h incubation with reactive oxygen species caused a significant increase in the integrated D-band to G-band ratio (Figure S11).

Hyperspectral NIR fluorescence microscopy was employed to study the intracellular fluorescence behavior of SWCNTs as a function of purity. Cells were again dosed with 1 mg  $\rm L^{-1}$  of unpurified- or purified-SWCNTs for 30 min, washed with 1xPBS, and then placed in 2 mL of fresh media for imaging. NIR fluorescence images were overlaid with transmitted light images to show the intracellular fluorescence response of both

SWCNT samples over the course of 24 h (Figure 3a). It was visually apparent that cells dosed with purified-SWCNTs exhibited higher fluorescence intensities as compared to the unpurified-SWCNT sample over a period of 24 h. To further investigate the fluorescence data, we plotted the normalized intensity per cell area against the (6,5)-SWCNT center wavelength for each cell (Figure 3b). We then separated the data sets by intensity and center wavelength to perform a statistical analysis as functions of sample purity and time (Figure 3c,d). It was observed that in addition to the purified-SWCNT sample being significantly brighter within cells, the (6,5)-SWCNT center wavelength was more homogeneous through time. This was in contrast to the unpurified-SWCNT sample, which showed not only a considerable decrease in its fluorescence intensity but also a heterogeneous population distribution in terms of wavelength shift amplitude and direction throughout all time points. After the initial 6 h period, it was observed that the purified-SWCNT sample was 45% brighter than the unpurified-SWCNT sample. Furthermore, substantial differences in the (6,5)-SWCNT center wavelength were observed in both samples due to their significantly different responses to the surrounding biomolecular environment. A blue shift of wavelength was seen for the purified-SWCNTs after 24 h, which we attribute to the presence of hydrophobic contents in the lysosomal lumen such as lipids. A significant red shift of wavelength was only observed in the unpurified-SWCNT sample, which we attribute to the state of aggregation of the sample over time and nonspecific binding of proteins on the nanotube surface.<sup>54</sup> We speculate that the decrease in fluorescence intensity through time for the unpurified-SWCNT sample was observed due to the presence of impurities and defect-laden SWCNTs which may lead to aggregation-induced quenching.<sup>55</sup> Finally, a long-term study with SWCNTs residing within cells for up to 168 h was conducted, and it was determined that the fluorescence intensity of both purified and unpurified samples diminishes at the same rate after 24 h (Figures S13 and S14).

Current solution-phase DNA-SWCNT biosensors exhibit highly stable fluorescence intensity and center wavelengths until an analyte is added, at which point optical modulations can be attributed to the disturbance in the system. <sup>21,56</sup> Moreover, current intracellular DNA-SWCNT biosensors rely on the instability of fluorescence intensity and center wavelengths as a function of time to explain biological phenomena and these optical modulations are attributed to specific pathways. <sup>16,54,57</sup> Here, we have developed an intracellular biosensor that has intrinsically stable fluorescence

intensity and center wavelength for up to 6 h. Generally, biological processes happen over minutes to hours, especially inside cells. Because there are no significant optical modulations over these first 6 h as a result of homeostatic cellular processes, any changes in fluorescence intensity or center wavelength can be directly attributed to an allostatic biological process, external disturbance, or stress placed on the cell. This purified-SWCNT platform has the potential to create more robust intracellular biosensors that are more closely related to solution-phase sensors, where stability is the expectation and any optical modulation from an intentional perturbance is significant.

An apoptosis-necrosis assay was performed to investigate the effects of the two SWCNT samples on the cell viability. In this experiment, RAW 264.7 murine macrophages were seeded on 35 mm glass-bottom microwell dishes and incubated for 24 h. After the first 24 h, the culture medium was spiked with either purified- or unpurified-SWCNTs and left in solution for an additional 24 h. Upon this continuous 24 h incubation with 1 mg L<sup>-1</sup> of either sample, there were no appreciable shifts in population distribution across the user-defined quadrants when compared to a control with no SWCNTs (Figure 4a). A bar graph representing the average percent distribution in each quadrant of the samples was prepared from the raw data sets used for the scatter plots (Figure 4b). It is evident that for the concentrations of SWCNTs used in this study ( $\leq 1$  mg L<sup>-1</sup>) there is limited apparent cytotoxicity in macrophage cells for either purified- or unpurified-SWCNTs.

In conclusion, we have identified a purification process that enhances the intracellular properties of DNA-SWCNTs while simultaneously improving multiple relevant parameters essential for developing the next generation of reliable and responsive carbon nanotube sensors for use in complex biological systems. We developed this sensor platform within macrophages, which have specialized uptake and accelerated lysosomal processing of foreign material compared to other cells. 43,59,60° First, hybrid stability within the cell is enhanced following the ATP purification process, which leads to measurements that are reproducible and generalizable across a range of intracellular incubation times. Second, optical signal stability is significantly increased via ATP purification, as purified-SWCNTs maintain their emission intensity and narrow center wavelength distribution. In contrast, an unpurified-SWCNT sample undergoes an unacceptably large decrease in emission intensity and bidirectional spread in the center wavelength. Combined, these two parameters address the most critical aspects for intracellular sensing: what is the degree of hybrid stability within a heterogeneous biological environment, and is the emission modulation of the sensor exclusively due to the presence of the analyte of interest?

We propose adoption of the process developed and validated in this work as the standard procedure for the preparation of SWCNTs for biological applications. Dispersing as-produced SWCNTs in surfactant provides high yields and is reproducible, and a standardized reference material is available for comparison. Surfactant-based ATP purification can remove all known classes of impurities, select for defect-free SWCNTs, and isolate single chiralities with a high selectivity. Complete exchange of the surfactant encapsulation for a biocompatible molecule of choice, for example ssDNA, has been achieved and validated in multiple biological applications. Finally, as evinced by this work, the purified-SWCNTs obtained from this process demonstrate superior optical stability and performance

in cells. As the field of engineered nanomaterial purification continues to progress at a staggering rate by yielding samples with increased purity and chiral specificity, 64–67 biological sensors developed with purified-SWCNTs will continue to outperform and outpace those made with unpurified-SWCNTs. Many issues associated with unpurified-SWCNTs are directly resolved via our proposed method of initially dispersing a SWCNT in a surfactant, performing surfactant-based aqueous two-phase purification, and integrating a biocompatible functionalization of choice via surfactant exchange, thus optimizing the engineered nanomaterial's performance for biomedical studies.

### ASSOCIATED CONTENT

# Supporting Information

The Supporting Information is available free of charge at https://pubs.acs.org/doi/10.1021/acs.nanolett.3c01727.

Experimental methods and materials, additional characterization spectra, images, and analysis (PDF)

## AUTHOR INFORMATION

# **Corresponding Author**

Daniel Roxbury — Department of Chemical Engineering, University of Rhode Island, Kingston, Rhode Island 02881, United States; oorcid.org/0000-0003-2812-3523; Email: roxbury@uri.edu

#### **Authors**

Aceer Nadeem — Department of Chemical Engineering, University of Rhode Island, Kingston, Rhode Island 02881, United States; orcid.org/0000-0002-5381-3561

Aidan Kindopp – Department of Chemical Engineering, University of Rhode Island, Kingston, Rhode Island 02881, United States

Ian Wyllie – Department of Chemical Engineering, University of Rhode Island, Kingston, Rhode Island 02881, United States

Lauren Hubert – Department of Chemical Engineering, University of Rhode Island, Kingston, Rhode Island 02881, United States

James Joubert — Department of Chemical Engineering, University of Rhode Island, Kingston, Rhode Island 02881, United States

Sophie Lucente – Department of Chemical Engineering, University of Rhode Island, Kingston, Rhode Island 02881, United States

Ewelina Randall – Molecular Pharmacology Program, Memorial Sloan Kettering Cancer Center, New York, New York 10065, United States

Prakrit V. Jena — Molecular Pharmacology Program, Memorial Sloan Kettering Cancer Center, New York, New York 10065, United States; Ocid.org/0000-0001-5493-3058

Complete contact information is available at: https://pubs.acs.org/10.1021/acs.nanolett.3c01727

## **Author Contributions**

A.N. and A.K. contributed equally to this work.

## Notes

The authors declare no competing financial interest.

## ACKNOWLEDGMENTS

This work was supported by the National Science Foundation (CAREER Award #1844536 and #2231621) and the University of Rhode Island College of Engineering. The confocal Raman data were acquired at the RI Consortium for Nanoscience and Nanotechnology, a URI College of Engineering core facility partially funded by the National Science Foundation EPSCoR, Cooperative Agreement #OIA-1655221. Research was made possible by the use of equipment available through the Rhode Island Institutional Development Award (IDeA) Network of Biomedical Research Excellence from the National Institute of General Medical Sciences of the National Institutes of Health under grant #P20GM103430 through the Centralized Research Core facility. Schematics were created using BioRender.com software.

# REFERENCES

- (1) Sharma, P.; Brown, S.; Walter, G.; Santra, S.; Moudgil, B. Nanoparticles for bioimaging. *Advances in colloid and interface science* **2006**, 123, 471–485.
- (2) Sun, E. Y.; Josephson, L.; Kelly, K. A.; Weissleder, R. Development of nanoparticle libraries for biosensing. *Bioconjugate Chem.* **2006**, *17* (1), 109–113.
- (3) Alim, S.; Vejayan, J.; Yusoff, M. M.; Kafi, A. Recent uses of carbon nanotubes & gold nanoparticles in electrochemistry with application in biosensing: A review. *Biosens. Bioelectron.* **2018**, *121*, 125–136.
- (4) Blanco, E.; Shen, H.; Ferrari, M. Principles of nanoparticle design for overcoming biological barriers to drug delivery. *Nature biotechnology* **2015**, 33 (9), 941–951.
- (5) Raffa, V.; Ciofani, G.; Vittorio, O.; Riggio, C.; Cuschieri, A. Physicochemical properties affecting cellular uptake of carbon nanotubes. *Nanomedicine* **2010**, *5* (1), 89–97.
- (6) Cai, P.; Leow, W. R.; Wang, X.; Wu, Y. L.; Chen, X. Programmable nano-bio interfaces for functional biointegrated devices. *Adv. Mater.* **2017**, 29 (26), 1605529.
- (7) Hirsch, A.; Vostrowsky, O. Functionalization of carbon nanotubes. *Functional molecular nanostructures* **2005**, 245, 193–237.
- (8) Pinals, R. L.; Yang, D.; Lui, A.; Cao, W.; Landry, M. P. Corona exchange dynamics on carbon nanotubes by multiplexed fluorescence monitoring. *J. Am. Chem. Soc.* **2020**, *142* (3), 1254–1264.
- (9) Barzegar, A.; Mansouri, A.; Azamat, J. Molecular dynamics simulation of non-covalent single-walled carbon nanotube functionalization with surfactant peptides. *Journal of Molecular Graphics and Modelling* **2016**, *64*, 75–84.
- (10) Hashida, Y.; Tanaka, H.; Zhou, S.; Kawakami, S.; Yamashita, F.; Murakami, T.; Umeyama, T.; Imahori, H.; Hashida, M. Photothermal ablation of tumor cells using a single-walled carbon nanotube—peptide composite. *Journal of controlled release* **2014**, *173*, 59–66.
- (11) Pradhan, B.; Kohlmeyer, R. R.; Setyowati, K.; Owen, H. A.; Chen, J. Advanced carbon nanotube/polymer composite infrared sensors. *Carbon* **2009**, *47* (7), 1686–1692.
- (12) Vaisman, L.; Wagner, H. D.; Marom, G. The role of surfactants in dispersion of carbon nanotubes. *Advances in colloid and interface science* **2006**, 128, 37–46.
- (13) Zhang, C.; Wang, P.; Barnes, B.; Fortner, J.; Wang, Y. Cleanly removable surfactant for carbon nanotubes. *Chem. Mater.* **2021**, 33 (12), 4551–4557.
- (14) Boghossian, A. A.; Zhang, J.; Barone, P. W.; Reuel, N. F.; Kim, J. H.; Heller, D. A.; Ahn, J. H.; Hilmer, A. J.; Rwei, A.; Arkalgud, J. R.; et al. Near-Infrared Fluorescent Sensors based on Single-Walled Carbon Nanotubes for Life Sciences Applications. *ChemSusChem* **2011**, *4* (7), 848–863.
- (15) Lefebvre, J.; Homma, Y.; Finnie, P. Bright band gap photoluminescence from unprocessed single-walled carbon nanotubes. *Physical review letters* **2003**, *90* (21), 217401.

- (16) Jena, P. V.; Roxbury, D.; Galassi, T. V.; Akkari, L.; Horoszko, C. P.; Iaea, D. B.; Budhathoki-Uprety, J.; Pipalia, N.; Haka, A. S.; Harvey, J. D.; et al. A carbon nanotube optical reporter maps endolysosomal lipid flux. ACS Nano 2017, 11 (11), 10689–10703.
- (17) Bachilo, S. M.; Strano, M. S.; Kittrell, C.; Hauge, R. H.; Smalley, R. E.; Weisman, R. B. Structure-assigned optical spectra of single-walled carbon nanotubes. *science* **2002**, 298 (5602), 2361–2366.
- (18) Yang, F.; Wang, M.; Zhang, D.; Yang, J.; Zheng, M.; Li, Y. Chirality pure carbon nanotubes: Growth, sorting, and characterization. *Chem. Rev.* **2020**, *120* (5), 2693–2758.
- (19) Nißler, R.; Kurth, L.; Li, H.; Spreinat, A.; Kuhlemann, I.; Flavel, B. S.; Kruss, S. Sensing with chirality-pure near-infrared fluorescent carbon nanotubes. *Anal. Chem.* **2021**, 93 (16), 6446–6455.
- (20) Roxbury, D.; Jena, P. V.; Williams, R. M.; Enyedi, B.; Niethammer, P.; Marcet, S.; Verhaegen, M.; Blais-Ouellette, S.; Heller, D. A. Hyperspectral microscopy of near-infrared fluorescence enables 17-chirality carbon nanotube imaging. *Sci. Rep.* **2015**, *5* (1), 1–6
- (21) Card, M.; Gravely, M.; M. Madani, S. Z.; Roxbury, D. A Spin-Coated Hydrogel Platform Enables Accurate Investigation of Immobilized Individual Single-Walled Carbon Nanotubes. *ACS Appl. Mater. Interfaces* **2021**, *13* (27), 31986–31995.
- (22) Ackermann, J.; Metternich, J. T.; Herbertz, S.; Kruss, S. Biosensing with Fluorescent Carbon Nanotubes. *Angew. Chem., Int. Ed.* **2022**, *61* (18), No. e202112372.
- (23) Galassi, T. V.; Jena, P. V.; Shah, J.; Ao, G.; Molitor, E.; Bram, Y.; Frankel, A.; Park, J.; Jessurun, J.; Ory, D. S.; et al. An optical nanoreporter of endolysosomal lipid accumulation reveals enduring effects of diet on hepatic macrophages in vivo. *Science translational medicine* **2018**, *10* (461), eaar2680.
- (24) Safaee, M. M.; Gravely, M.; Roxbury, D. A wearable optical microfibrous biomaterial with encapsulated nanosensors enables wireless monitoring of oxidative stress. *Adv. Funct. Mater.* **2021**, *31* (13), 2006254.
- (25) Yamada, K.; Kim, C.-T.; Kim, J.-H.; Chung, J.-H.; Lee, H. G.; Jun, S. Single walled carbon nanotube-based junction biosensor for detection of Escherichia coli. *PLoS One* **2014**, *9* (9), No. e105767.
- (26) Salzmann, C. G.; Llewellyn, S. A.; Tobias, G.; Ward, M. A.; Huh, Y.; Green, M. L. The role of carboxylated carbonaceous fragments in the functionalization and spectroscopy of a single-walled carbon-nanotube material. *Adv. Mater.* **2007**, *19* (6), 883–887.
- (27) Kiciński, W.; Dyjak, S. Transition metal impurities in carbon-based materials: Pitfalls, artifacts and deleterious effects. *Carbon* **2020**, *168*, 748–845.
- (28) Cui, H.-F.; Vashist, S. K.; Al-Rubeaan, K.; Luong, J. H.; Sheu, F.-S. Interfacing carbon nanotubes with living mammalian cells and cytotoxicity issues. *Chemical research in toxicology* **2010**, 23 (7), 1131–1147.
- (29) Liu, B.; Wu, F.; Gui, H.; Zheng, M.; Zhou, C. Chirality-controlled synthesis and applications of single-wall carbon nanotubes. *ACS Nano* **2017**, *11* (1), 31–53.
- (30) Albertsson, P.-Å. Partition of cell particles and macromolecules in polymer two-phase systems. *Advances in protein chemistry* **1970**, *24*, 309–341.
- (31) Asenjo, J. A.; Andrews, B. A. Aqueous two-phase systems for protein separation: a perspective. *Journal of Chromatography A* **2011**, 1218 (49), 8826–8835.
- (32) Iqbal, M.; Tao, Y.; Xie, S.; Zhu, Y.; Chen, D.; Wang, X.; Huang, L.; Peng, D.; Sattar, A.; Shabbir, M. A. B.; et al. Aqueous two-phase system (ATPS): an overview and advances in its applications. *Biological procedures online* **2016**, *18* (1), 1–18.
- (33) Hatti-Kaul, R. Aqueous two-phase systems. *Molecular biotechnology* **2001**, *19* (3), 269–277.
- (34) Soares, R. R.; Azevedo, A. M.; Van Alstine, J. M.; Aires-Barros, M. R. Partitioning in aqueous two-phase systems: Analysis of strengths, weaknesses, opportunities and threats. *Biotechnology journal* **2015**, *10* (8), 1158–1169.

- (35) Pereira, J. F.; Freire, M. G.; Coutinho, J. A. Aqueous two-phase systems: Towards novel and more disruptive applications. *Fluid Phase Equilib.* **2020**, *505*, 112341.
- (36) Subbaiyan, N. K.; Parra-Vasquez, A. N. G.; Cambré, S.; Cordoba, M. A. S.; Yalcin, S. E.; Hamilton, C. E.; Mack, N. H.; Blackburn, J. L.; Doorn, S. K.; Duque, J. G. Bench-top aqueous two-phase extraction of isolated individual single-walled carbon nanotubes. *Nano Research* **2015**, *8* (5), 1755–1769.
- (37) Ao, G.; Khripin, C. Y.; Zheng, M. DNA-Controlled Partition of Carbon Nanotubes in Polymer Aqueous Two-Phase Systems. *J. Am. Chem. Soc.* **2014**, *136* (29), 10383–10392.
- (38) Lyu, M.; Meany, B.; Yang, J.; Li, Y.; Zheng, M. Toward complete resolution of DNA/carbon nanotube hybrids by aqueous two-phase systems. *J. Am. Chem. Soc.* **2019**, *141* (51), 20177–20186.
- (39) Li, H.; Gordeev, G.; Garrity, O.; Reich, S.; Flavel, B. S. Separation of small-diameter single-walled carbon nanotubes in one to three steps with aqueous two-phase extraction. *ACS Nano* **2019**, *13* (2), 2567–2578.
- (40) Nißler, R.; Bader, O.; Dohmen, M.; Walter, S. G.; Noll, C.; Selvaggio, G.; Groß, U.; Kruss, S. Remote near infrared identification of pathogens with multiplexed nanosensors. *Nat. Commun.* **2020**, *11* (1), 1–12.
- (41) Bhattacharya, S.; Roxbury, D.; Gong, X.; Mukhopadhyay, D.; Jagota, A. DNA Conjugated SWCNTs Enter Endothelial Cells via Rac1Mediated Macropinocytosis. *Nano Lett.* **2012**, *12* (4), 1826–1830.
- (42) Gravely, M.; Safaee, M. M.; Roxbury, D. Biomolecular functionalization of a nanomaterial to control stability and retention within live cells. *Nano Lett.* **2019**, *19* (9), 6203–6212.
- (43) Gravely, M.; Roxbury, D. Multispectral Fingerprinting Resolves Dynamics of Nanomaterial Trafficking in Primary Endothelial Cells. *ACS Nano* **2021**, *15* (7), 12388–12404.
- (44) Qiao, Y.; Zhao, R.; Zhang, M.; Zhang, H.; Wang, Y.; Hu, P. Phenylboronic acid derivative-modified (6,5) single-wall carbon nanotube probes for detecting glucose and hydrogen peroxide. *RSC Adv.* **2019**, 9 (4), 2258–2267.
- (45) Khripin, C. Y.; Tu, X.; Howarter, J.; Fagan, J.; Zheng, M. Concentration Measurement of Length-Fractionated Colloidal Single-Wall Carbon Nanotubes. *Anal. Chem.* **2012**, *84* (20), 8733–8739.
- (46) Zheng, M.; Diner, B. A. Solution Redox Chemistry of Carbon Nanotubes. *J. Am. Chem. Soc.* **2004**, *126* (47), 15490–15494.
- (47) Zhang, D.; Yang, J.; Li, Y. Spectroscopic Characterization of the Chiral Structure of Individual Single-Walled Carbon Nanotubes and the Edge Structure of Isolated Graphene Nanoribbons. *Small* **2013**, *9* (8), 1284–1304.
- (48) Ghosh, S.; Bachilo, S. M.; Simonette, R. A.; Beckingham, K. M.; Weisman, R. B. Oxygen Doping Modifies Near-Infrared Band Gaps in Fluorescent Single-Walled Carbon Nanotubes. *Science* **2010**, 330 (6011), 1656–1659.
- (49) Liu, Z.; Davis, C.; Cai, W.; He, L.; Chen, X.; Dai, H. Circulation and long-term fate of functionalized, biocompatible single-walled carbon nanotubes in mice probed by Raman spectroscopy. *Proc. Natl. Acad. Sci. U. S. A.* **2008**, *105* (5), 1410–1415.
- (50) Dillon, A. C.; Yudasaka, M.; Dresselhaus, M. S. Employing Raman spectroscopy to qualitatively evaluate the purity of carbon single-wall nanotube materials. *J. Nanosci Nanotechnol* **2004**, *4* (7), 691–703.
- (51) Dillon, A. C.; Parilla, P. A.; Alleman, J. L.; Gennett, T.; Jones, K. M.; Heben, M. J. Systematic inclusion of defects in pure carbon single-wall nanotubes and their effect on the Raman D-band. *Chem. Phys. Lett.* **2005**, *401* (4), 522–528.
- (52) Kagan, V. E.; Konduru, N. V.; Feng, W.; Allen, B. L.; Conroy, J.; Volkov, Y.; Vlasova, I. I.; Belikova, N. A.; Yanamala, N.; Kapralov, A.; Tyurina, Y. Y.; Shi, J.; Kisin, E. R.; Murray, A. R.; Franks, J.; Stolz, D.; Gou, P.; Klein-Seetharaman, J.; Fadeel, B.; Star, A.; Shvedova, A. A. Carbon nanotubes degraded by neutrophil myeloperoxidase induce less pulmonary inflammation. *Nat. Nanotechnol* **2010**, *5* (5), 354–9.

- (53) He, X.; White, D. L.; Kapralov, A. A.; Kagan, V. E.; Star, A. Photoluminescence Response in Carbon Nanomaterials to Enzymatic Degradation. *Anal. Chem.* **2020**, 92 (19), 12880–12890.
- (54) Naumov, A. V.; Ghosh, S.; Tsyboulski, D. A.; Bachilo, S. M.; Weisman, R. B. Analyzing Absorption Backgrounds in Single-Walled Carbon Nanotube Spectra. *ACS Nano* **2011**, 5 (3), 1639–1648.
- (55) Gravely, M.; Kindopp, A.; Hubert, L.; Card, M.; Nadeem, A.; Miller, C.; Roxbury, D. Aggregation Reduces Subcellular Localization and Cytotoxicity of Single-Walled Carbon Nanotubes. *ACS Appl. Mater. Interfaces* **2022**, *14* (17), 19168 19177.
- (56) Kruss, S.; Landry, M. P.; Vander Ende, E.; Lima, B. M. A.; Reuel, N. F.; Zhang, J.; Nelson, J.; Mu, B.; Hilmer, A.; Strano, M. Neurotransmitter Detection Using Corona Phase Molecular Recognition on Fluorescent Single-Walled Carbon Nanotube Sensors. *J. Am. Chem. Soc.* **2014**, *136* (2), 713–724.
- (57) Kelich, P.; Jeong, S.; Navarro, N.; Adams, J.; Sun, X.; Zhao, H.; Landry, M. P.; Vuković, L. Discovery of DNA–Carbon Nanotube Sensors for Serotonin with Machine Learning and Near-infrared Fluorescence Spectroscopy. *ACS Nano* **2022**, *16* (1), 736–745.
- (58) Cadart, C.; Venkova, L.; Recho, P.; Lagomarsino, M. C.; Piel, M. The physics of cell-size regulation across timescales. *Nat. Phys.* **2019**, *15* (10), 993–1004.
- (59) Vieira, O. V.; Botelho, R. J.; Grinstein, S. Phagosome maturation: aging gracefully. *Biochem. J.* **2002**, *366* (3), *689*–704.
- (60) Huotari, J.; Helenius, A. Endosome maturation. *EMBO Journal* **2011**, *30* (17), 3481–3500.
- (61) Kim, M.; Chen, C.; Yaari, Z.; Frederiksen, R.; Randall, E.; Wollowitz, J.; Cupo, C.; Wu, X.; Shah, J.; Worroll, D.; Lagenbacher, R. E.; Goerzen, D.; Li, Y.-M.; An, H.; Wang, Y.; Heller, D. A. Nanosensor-based monitoring of autophagy-associated lysosomal acidification in vivo. *Nat. Chem. Biol.* **2023**, DOI: 10.1038/s41589-023-01364-9.
- (62) Ackermann, J.; Stegemann, J.; Smola, T.; Reger, E.; Jung, S.; Schmitz, A.; Herbertz, S.; Erpenbeck, L.; Seidl, K.; Kruss, S. High Sensitivity Near-Infrared Imaging of Fluorescent Nanosensors. *Small* **2023**, *19* (14), 2206856.
- (63) Langenbacher, R.; Budhathoki-Uprety, J.; Jena, P. V.; Roxbury, D.; Streit, J.; Zheng, M.; Heller, D. A. Single-Chirality Near-Infrared Carbon Nanotube Sub-Cellular Imaging and FRET Probes. *Nano Lett.* **2021**, *21* (15), 6441–6448.
- (64) Li, H.; Sims, C. M.; Kang, R.; Biedermann, F.; Fagan, J. A.; Flavel, B. S. Isolation of the (6,5) single-wall carbon nanotube enantiomers by surfactant-assisted aqueous two-phase extraction. *Carbon* **2023**, 204, 475–483.
- (65) Podlesny, B.; Hinkle, K. R.; Hayashi, K.; Niidome, Y.; Shiraki, T.; Janas, D. Highly-Selective Harvesting of (6,4) SWCNTs Using the Aqueous Two-Phase Extraction Method and Nonionic Surfactants. *Advanced Science* **2023**, *10* (14), 2207218.
- (66) Luo, X.; Wei, X.; Liu, L.; Yao, Z.; Xiong, F.; Zhou, W.; Xie, S.; Liu, H. One-step separation of high-purity single-chirality single-wall carbon nanotubes using sodium hyodeoxycholate. *Carbon* **2023**, 207, 129–135
- (67) Tiwari, P.; Podleśny, B.; Krzywiecki, M.; Milowska, K. Z.; Janas, D. Understanding the partitioning behavior of single-walled carbon nanotubes using an aqueous two-phase extraction system composed of non-ionic surfactants and polymers. *Nanoscale Horizons* **2023**, 8 (5), 685–694.